Nano Research

Open Access

Research Article

Enhancing performance of fullerene-based organic electrochemical transistors via side-chain engineering

Wenxin Fang[1,§], Zijie Li[2,§], Chengdong Wang[1,§], Xiaowei Zhao[1], Junyu Li[3], Gang Ye[4], Fengwei Huo[5], Li Qiu[2] ✉, Yanxi Zhang[1] ✉, and Wei Huang[6] ✉

[1] *Institute of Flexible Electronics (IFE, Future Technologies), Xiamen University, Xiamen 361005, China*
[2] *Yunnan Key Laboratory of Electromagnetic Materials and Devices, National Center for International Research on Photoelectric and Energy Materials, School of Materials and Energy, Yunnan University, Kunming 650091, China*
[3] *Sinopec Shanghai Research Institute of Petrochemical Technology, Shanghai 201028, China*
[4] *Key Laboratory for the Green Preparation and Application of Functional Materials, Hubei Key Laboratory of Polymer Materials, School of Materials Science and Engineering, Hubei University, Wuhan 430062, China*
[5] *Key Laboratory of Flexible Electronics (KLOFE) & Institute of Advanced Materials (IAM), Jiangsu National Synergetic Innovation Center for Advanced Materials (SICAM), Nanjing Tech University (NanjingTech), Nanjing 211800, China*
[6] *Frontiers Science Center for Flexible Electronics, MIIT Key Laboratory of Flexible Electronics (KLoFE), Northwestern Polytechnical University, Xi'an 710072, China*
§ *Wenxin Fang, Zijie Li, and Chengdong Wang contributed equally to this work.*

Cite this article: *Nano Research*, **2025**, *18*, 94907149. https://doi.org/10.26599/NR.2025.94907149

ABSTRACT: The performance of organic electrochemical transistors (OECTs) relies on the interaction between organic semiconductors and ions. Consequently, hydrophilic ethylene glycol (EG) side chains are incorporated into organic semiconductors to improve the channel's capacity to absorb ions. However, the EG substituted organic semiconductors tend to swell when immersed in aqueous electrolytes and exhibit microstructural changes induced by dopant ions. In our research, we introduce an alkyl spacer to create distance between the fullerene and EG chain. This approach is designed to reduce the negative effects of swelling and balance the ion and electron conduction. We conducted an analysis of OECTs using four fullerene derivatives: no alkyl spacer, butyl, hexyl, and octyl spacers. The OECTs based on fullerene derivatives with butyl and hexyl spacers exhibit enhanced transconductance (g_m = 11.8 and 19.4 mS) compared to the ones without alkyl spacers. It has also been observed that the butyl and hexyl spacers lead to a more than tenfold increase in volumetric capacitance. Further increasing the alkyl spacer (octyl group) leads to no transistor behavior. Our study uncovers the relationship between alkyl spacers and the performance of OECTs based on fullerene derivatives. This will serve as a guideline for designing n-type small molecules for OECTs. Finally, we showcased the potential of utilizing OECTs based on these fullerene derivatives in cation sensing, which is promising for developing sweat sensors.

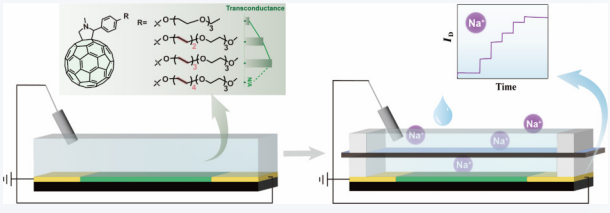

KEYWORDS: organic electrochemical transistors, fullerene derivatives, ethylene glycol side chains, ion and electron conduction

1 Introduction

Organic electrochemical transistors (OECTs) have garnered widespread attention due to their potential applications in areas such as neuromorphic sensing, perception, and computing [1–3]. OECTs present numerous advantages compared to silicon-based transistors, including lower operating voltages, high sensitivity to ions and biomolecules, and the capacity to be manufactured as flexible electronics. Researches on organic mixed ionic-electronic conductors (OMIECs) [4] have focused on electronic transport in the context of delocalized π-conjugated polymers, which are responsive to ions in the electrolyte and then conduct electrons via carrier hopping between chains. OECTs using OMIECs as channel materials are electrochemical devices with an emerging bio-like operating mechanism. OECTs are a three-terminal device with a gate electrode, a source electrode, and a drain electrode. The gate voltage, V_G, drives ions to migrate from the electrolyte into the

Received: September 30, 2024; **Revised:** November 1, 2024
Accepted: November 25, 2024

✉Address correspondence to Wei Huang, iamwhuang@nwpu.edu.cn; Yanxi Zhang, ifeyxzhang@xmu.edu.cn; Li Qiu, qiuli@ynu.edu.cn

OMIECs to compensate for the electron charge, which changes the channel conductance via electrochemical oxidation or reduction reaction [5]. During this process, ions could reversibly dope into and launched from the bulk of the material. OECTs can amplify small gate potential changes into significant current modulations, making them ideal for trace substance detection or circuit signal amplification. In addition, the conduction mechanism enables OECTs to be applied in organisms in the most biologically relevant operation mode for transmitting signals across biological and non-biological interfaces or simulating biological functions [6]. OECTs have a low operating voltage, a biologically-like ion-electron conduction mechanism, good biocompatibility, and other application advantages. As an excellent artificial device for human-computer interaction, it is currently applied in, for example, artificial synapses [7–10] and artificial neurons [11–13].

An important indicator for evaluating the OECT performance is the transconductance g_m, which can be extracted from the linear region of the transfer curve by $\partial I_D/\partial V_G$. The g_m quantifies the amplification factor and is determined by the combination of channel size and material intrinsic characteristics according to Eq. (1) [14]

$$g_m = \mu C^* W d/L|V_{th} - V_G| \quad (1)$$

where μ is the carrier mobility, C^* is the volumetric capacitance of the material, W is the channel width, L is the channel length, d is the film thickness, and V_{th} is the threshold voltage for OECTs. Maximum transconductance g_{max} is often employed to compare the signal amplification performance of different devices. To eliminate the influence of channel size on the evaluation of material performance, μC^* was utilized as the merit value of channel materials. Due to the aqueous system of poly(3,4-ethylenedioxythiophene):poly(styrene sulfonate) (PEDOT:PSS), stable performance and higher μC^* values make it widely used as an active layer for OECTs. However, since PEDOT:PSS OECTs operate in depletion mode, it is necessary to apply V_G to turn off the devices. Moreover, the quiescent power consumption is high, so it is necessary to develop the OECTs that operate in enhanced mode [15]. By molecularly designing the backbone and side chains [16–20], conjugated polymers achieve better and more stable performance than PEDOT:PSS. P-type OECTs are being widely developed, which is an order of magnitude higher in performance than the best n-type counterparts [21, 22]. N-type OECTs have been applied in various fields [23–25], but their performance remains a limiting factor. The main reason limiting the development of n-type OMIECs is their instability in aqueous environments and air. However, complex logic circuits [26], and biosensing [27], urgently require high-performance n-type organic semiconductor materials. Recently, it has been shown that the OECT performance is improved by substituting hydrophobic alkyl chains with hydrophilic glycol side chains [28], or inserting alkyl units into glycol chains [20].

Although the side-chain engineering strategy in materials has significantly improved the performance of conjugated polymer-based OECTs [20, 29, 30], n-type conjugated polymers have always faced the problem of low electron mobility [31]. Small semiconducting molecules are usually better crystallized, facilitating carrier transport within the bulk of the material. They have an overall electron mobility one order of magnitude higher than that of conjugated polymers [32], and, thus, can serve as promising active layers for OECTs. In addition, organic small molecules have the advantage over polymers in that they are easy to synthesize and purify and have less influence from batch to batch. However, at the same time, there are fewer doping sites within the bulk, ion doping becomes more difficult.

Fullerenes are fascinating materials for electronics due to their efficient electron transport. Since fullerenes are insoluble, researchers have used side-chain modifications to obtain fullerene derivatives, a class of small-molecule receptors with excellent performance [33]. Although fullerene derivatives have long been used as active layers of OFETs, there have been few studies on fullerene derivatives based OECT. Bischak et al. used C60-TEG, a fullerene derivative of the glycosylated side chain, as the active layer of OECT for the first time [34]. C60-TEG has a great performance improvement compared to PCBM. Stein et al. successfully fabricated ambipolar OECTs by blending PrC60MA with p(g2T-TT) [35]. The work of Bischak et al. is very constructive; they show that many of the design rules for conjugated polymers are suitable for small molecule n-type semiconductors. However, this is not enough, and many previous studies have revealed the effects of different ratios of EG and alkyl on OECT performance and the trade-off relationship between C^* and μ [20, 29, 30]. It is necessary to explore the properties of fullerene derivative OECT further.

The OECT mechanism requires that its materials facilitate the entry and ejection of ions. Oligomeric ethylene glycol (OEG) has good hydrophilic properties, and introducing OEG into the side chain is commonly used to improve the hydrophilic and ion-permeable properties of OECT materials. The hydrophilic side chains ensure the doping and storage of ions in the bulk of the material [36]. In an electrochemical cycle, the material immersed in the electrolyte undergoes passive and active swelling. Doping and dedoping by hydrated ions from the electrolyte disrupts the internal buildup of the material. Excessive swelling leads to the disruption of electronic pathways in OECT materials, and the introduction of side chains in alkyl units can inhibit passive swelling and thus improve OECT performance. Alkyl units of different lengths are inserted into the side chains of fullerene spheres to obtain optimal performance.

In this study, we investigate fullerene derivatives functioned with hybrid alkyl-glycol side chains as active layers for n-type OECTs (Fig. 1(a)) and explore how the alkyl spacers affect the mixed ionic-electronic conduction properties. The detailed synthesis of the molecules is given in the Electronic Supplementary Material (ESM). We introduce the alkyl units to form amphiphilic side chains for comparison with the EG-substituted fullerene derivative (PTEG1). The fullerene derivatives comprising butyl (PC4TEG), hexyl (PC6TEG), and octyl spacers (PC8TEG) are shown in Fig. 1(b). The results demonstrate that the appropriate alkyl spaces could effectively enhance the volumetric capacitance and ion diffusion capacity of fullerene derivatives. PC6TEG has the highest volumetric capacitance among all four molecules, which is 569.49 F·cm^{-3}. PC4TEG exhibits approximately twice the ion diffusion capacity of other materials. OECTs based on PC8TEG with the longest alkyl spacers are unable to switch on within the water's potential window. The response of PC4TEG-based OECTs to Na^+ proves the potential of n-type OMIECs for cation sensing applications. This study aims to demonstrate that embedding proper alkyl spacers into EG side chains can effectively improve the performance of fullerene-based n-type OECTs.

2 Results and discussion

Four fullerene derivatives are used as the channel material for OECTs, and the device structure of OECTs is shown in Fig. 1. 0.1 M NaCl is used as the electrolyte. The atomic force microscopy

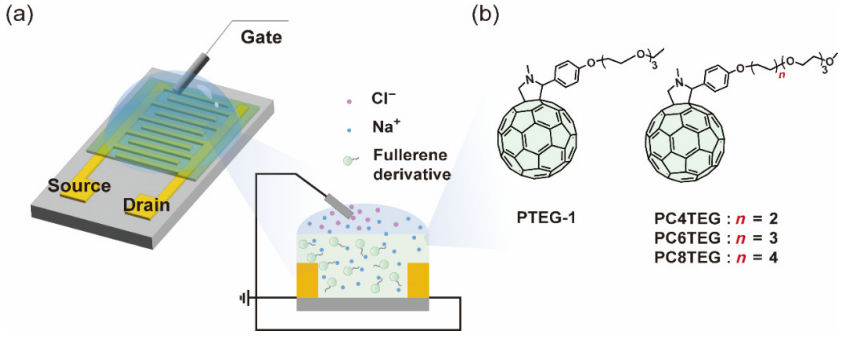

Figure 1 (a) Schematic of OECTs. (b) Chemical structure of fullerene derivatives: PTEG-1, PC4TEG, PC6TEG, and PC8TEG.

(AFM) of four fullerene derivatives before and after doping is shown in Fig. S20 in the ESM. The OECTs are characterized by the transfer curves (where V_D is fixed, recording I_D versus V_G) and the output curves (I_D versus V_D at different V_G values). The devices could not be turned on within the operation voltage when PC8TEG is used as the channel material of OECTs, and its transfer and output curves are shown in Figs. S13(c) and S13(d) in the ESM. Since PC8TEG has the most extended alkyl unit, we hypothesize that its hydrophobic nature hinders Na^+ ions from approaching the bulky fullerene balls and doping them. The output curves of OECTs based on PTEG-1, PC4TEG, and PC6TEG (Fig. S14 in the ESM) indicate that all devices have reached the saturation region at V_D = 0.6 V. Therefore, the transfer curve for the saturation region is recorded at V_D = 0.6 V (Fig. 2(a) and Fig. S13(b) in the ESM). The PTEG-1, PC4TEG, and PC6TEG based OECTs all exhibit n-type enhancement operation. OECTs with PC4TEG and PC6TEG achieve an on-off ratio exceeding three orders of magnitudes. The trends of V_{th} and g_m can be visualized in Fig. 3(a). PTEG-1 with only EG side chains has the lowest g_m, resulting from its highest threshold voltage V_{th} and lowest μC^* (see Table 1 and Fig. S19 in the ESM). PC4TEG OECTs have the lowest threshold voltage, in contrast to PC6TEG OECTs, which have a slightly higher V_{th} and g_m (up to 30 mS for all devices). The parameters of OECTs are summarized in Table 1.

The ions are injected from aqueous electrolyte into OMIECs, so the ionic-electronic coupling depends on the hydrophobic nature of the material. The film's water contact angles exhibit the trend in hydrophilicity of these four molecules, as shown in Fig. S10 in the ESM. From PTEG-1 to PC8TEG, the water contact angles show a gradual increase with the extension of the alkyl unit; they are 64.8°, 68.5°, 71.4°, and 75.4°, respectively. The material with smaller contact angle is more hydrophilic, making it more favorable for ions to penetrate. The fullerene derivatives are spin-coated on indium tin oxide (ITO) as the working electrode and placed in 0.1 M NaCl solution for cyclic voltammetry (CV) scanning. The results are shown in Fig. S11 in the ESM. During the CV experiments, electrons transfer between the active film and ITO electrode, causing Na^+ in the electrolyte to migrate to compensate for the charge. The CV plots show that the fullerene derivatives can be reversibly reduced and oxidized. The reduction potentials of the materials can be extracted from the CV plots (trend plot in Fig. 3(b)), which indicates the ease with which Na^+ can electrochemically dope the materials in solution. The trend in reduction potential aligns with the OECT threshold voltage of the fullerene derivatives. Both PTEG-1, which contains hydrophilic EG side chains, and PC8TEG, which contains the most extended alkyl unit, have the highest reduction potential onset (–0.51 V). These reduction potential onsets indicate that PTEG-1 and PC8TEG are more difficult to be doped in an aqueous solution than PC4TEG and PC6TEG.

To monitor the ion doping process of the fullerene derivatives at various voltages, we conduct spectroelectrochemical tests in a 0.1 M NaCl solution. The tests are performed using ITO coated with a fullerene film as the working electrode, which is immersed in the solution. Figure S12 in the ESM shows the absorption spectra of the four materials as a function of applied bias (vs. Ag/AgCl). All the fullerene derivatives exhibit minimal change within the scanning range of wavelengths with applied bias. Only PC6TEG displays a slight increase in the visible range, consistent with the previous study on C60-TEG [34]. This suggests that the doping of PC6TEG with Na^+ OECTs is the most effective among all four materials. The transient response is tested by applying a square wave pulse V_G = 0 to 1 V to the gate, recording the change in I_D over time, and then fitting the device's turn-on and turn-off response times with an exponential function. Figure 3(a) and Fig. S15 in the ESM show that OECTs based on PC4TEG have the fastest turn-on response (τ_{on} = 21.6 ms, τ_{off} = 1.9 ms), followed by the PTEG-1 (τ_{on} = 36.7 ms, τ_{off} = 3.5 ms), while the PC6TEG have the slowest turn-on

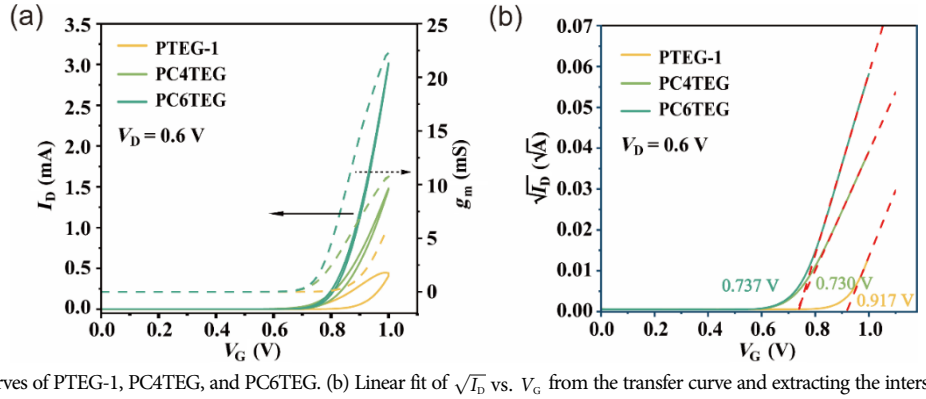

Figure 2 (a) Transfer curves of PTEG-1, PC4TEG, and PC6TEG. (b) Linear fit of $\sqrt{I_D}$ vs. V_G from the transfer curve and extracting the intersection of the fit linear and $\sqrt{I_D}$ = 0 to get the threshold voltage V_{th}. The V_{th} of PTEG-1, PC4TEG, and PC6TEG were 0.917, 0.730, and 0.737 V.

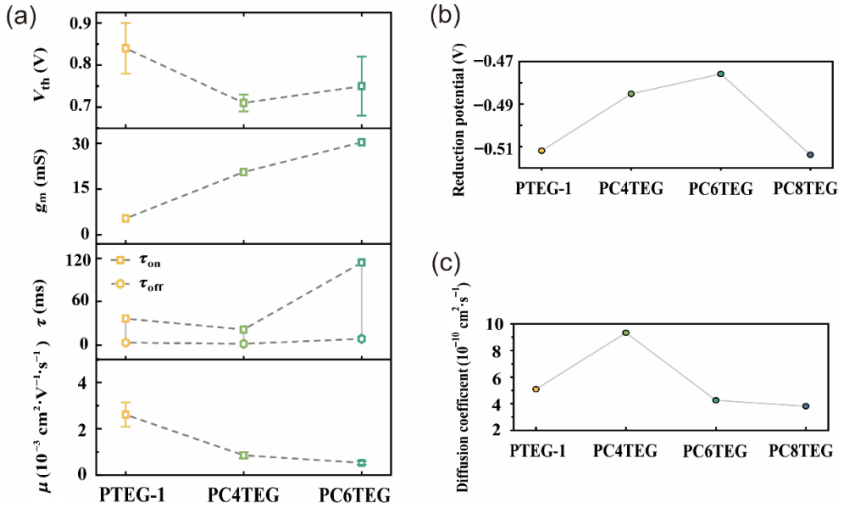

Figure 3 (a) V_{th}, g_m, τ and μ extracted from OECTs data of four fullerene derivatives. (b) The reduction potential of all fullerene film extracted from CV in 0.1 M NaCl(aq). (c) Ion diffusion coefficient of all fullerene film extracted from chronoamperometry measurements.

Table 1 The summary of steady-state OECT based on fullerene derivatives, four devices were measured for each fullerene derivative to extract the standard deviation

Fullerene derivative	V_{th} (V)	g_m (mS)	μC^* (F·V^{-1}·cm^{-1}·s^{-1})	μ (10^{-3} cm^2·V^{-1}·s^{-1})	C^* (F·cm^{-3})	$I_{on/off}$
PTEG-1	0.84 ± 0.06	4.6 ± 0.8	0.104 ± 0.021	2.61 ± 0.528	39.78	> 10^2
PC4TEG	0.71 ± 0.02	11.8 ± 8.8	0.347 ± 0.054	0.853 ±0.133	406.77	> 10^3
PC6TEG	0.75 ± 0.07	19.4 ± 11	0.300 ± 0.045	0.527 ± 0.079	569.49	> 10^3
PC8TEG	N/A	N/A	N/A	N/A	N/A	N/A

response (τ_{on} = 114.3 ms, τ_{off} = 8.8 ms). The sequence of device response speed from highest to lowest is as follows: PC4TEG > PTEG-1 > PC6TEG.

OECTs consist of two conducting pathways: ionic conduction (between the electrolyte and the channel) and electronic conduction (between the source and drain) [15]. The switching speed of OECTs can be influenced by the rate of ion diffusion within the electrolyte and channel material and the rate of electron transport between source and drain. However, the electron velocity is significantly faster than the ion migration within the electrolyte and diffusion within the material. Hence, ion diffusion is a key factor limiting the device's operating speed. In Fig. 3(c) and Fig. S17 in the ESM, the ion diffusion coefficients of these four fullerene materials are extracted using chronoamperometry. The result follows the order: PC4TEG > PTEG-1 > PC6TEG > PC8TEG. The trend of ion diffusion aligns with the device's transient response, indicating that the ion diffusion correlates with the device's operation speed. Inserting the proper alkyl spacer, like butyl (C4), favors ion diffusion. Furthermore, we speculate that the inserted alkyl unit extends the distance between the induced electrons on C_{60} and the cations on the EG side chains. The electrostatic interaction force between Na^+ and electrons on C_{60} is inversely proportional to the distance. When the distance between the two is short, this strong Coulombic force reduces the number of free charges [37]. The extended distance of PC4TEG weakens the ion-electron interaction force, resulting in faster ion diffusion. However, the ion diffusion coefficients decrease significantly as the hydrophobicity of PC6TEG and PC8TEG affects the ions.

The volumetric capacitance (C^*) is determined using electrochemical impedance spectroscopy (EIS) at an offset potential of –0.8 V vs. Ag/AgCl in a 0.1 M NaCl aqueous solution. We use Kovac's circuit to fit the capacitance values of PTEG-1, PC4TEG, and PC6TEG, and normalize the capacitance by volume (Table S1 in the ESM). The double peaks in the phase angle plot indicate the presence of two capacitances within the system [30], which originate from the flat plate capacitance at the electrolyte-channel interface and the bulk capacitance of the channel material [38]. Instead of a pure capacitive element, we use an equivalent circuit with two capacitive elements, CPE1 and CPE2, and a constant phase element, CPE, because the system is more complicated than an ideal capacitor. The phase peaks corresponding to CPE2 occur in the 1 to 10 Hz, and those corresponding to CPE1 in the 10^3 to 10^4 Hz. The CPE2 capacitance values of all materials are higher than the CPE1 capacitance values, which is in line with the characteristics of bulk and flat plate capacitance. In Fig. S18 in the ESM, the capacitance C represents the corresponding volumetric capacitance value of CPE2 from the equivalent circuit. PC6TEG shows the highest C^* at 569.49 F·cm^{-3}, and both PC4TEG and PC6TEG have C^* values more than ten times higher than PTEG-1. The volumetric capacitance values of the materials, C^*, follow the same trend as the OECT transconductance values, further confirming the enhancement of ionic doping into the bulk by introducing a butyl or hexyl spacer.

To investigate the impact of alkyl spacers on the micro structure, we utilize grazing incidence wide angle X-ray scattering (GIWAXS) to characterize the thin film morphology of these four fullerene derivatives, as depicted in Fig. 4. The narrow arc-like signals indicate all samples have a high degree of crystal orientation across the entire film. Three reflection peaks ((00l), l = 1, 2, 3) can be seen in the out-of-plane q_z direction (Fig. 4(b)), indicating that these fullerene derivatives form a layered structure along the normal direction of the substrate. The d-spacing is 2.4 nm for PTEG-1, 2.8 nm for PC4TG, 3.3 nm for PC6TEG, and 2.6 nm for PC8TEG. As the (001) peaks move toward lower q values, the d-spacing increases, which is possibly more favorable for the penetration of hydronium ions into the bulk of materials. When the alkyl unit is

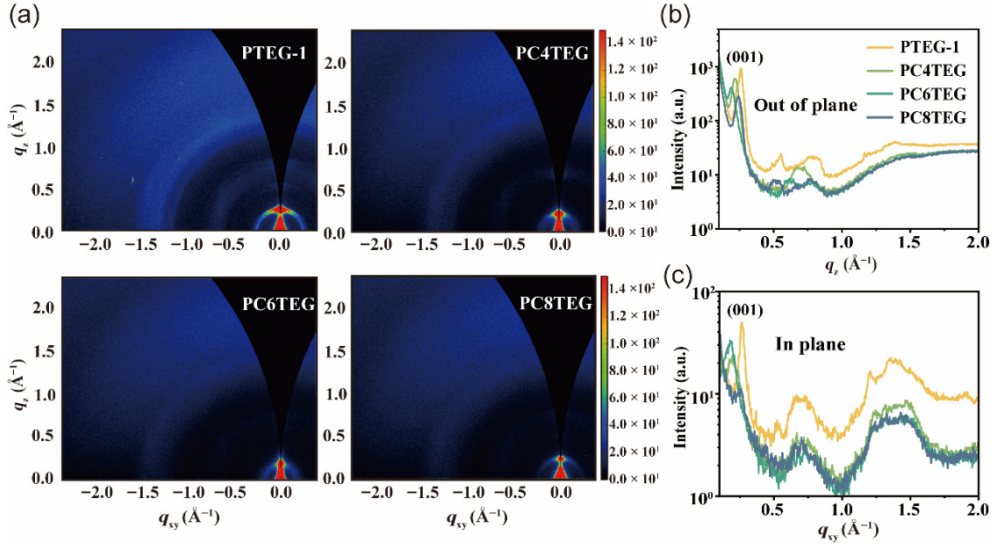

Figure 4 (a) 2D GIWAXS patterns of PTEG-1, PC4TEG, PC6TEG, and PC8TEG. (b) The out-of-plane and (c) in-plane line cuts of each fullerene derivative.

further increased, the (001) peak of PC8TEG shifts to lower q values, and the d-spacing decreases. The internal order of the material increases, and due to its hydrophobic nature, the OECTs based on PC8TEG exhibit difficulty turning on within the potential window. Molecular arrangement affects the formation of ion transport pathways. When the crystal face spacing is moderate, it is conducive to forming continuous and stable ion channels so ions can be efficiently transported [4]. In general, the larger the spacing between crystal faces, the easier the ion migration [29]. This is because larger crystal face spacing can provide more space for ions to move, reducing interactions and collisions between ions and thus reducing energy loss during migration. This explains the substantial increase in OECT's g_m, $I_{on/off}$, for PC4TEG and PC6TEG compared with PTEG-1. However, it must be noted that the movement of ions within the OECT channel is a complex process, and this study attempts to give a preliminary outline of the performance changes of the four materials with GIWAXS data.

Ions are indispensable for energy conversion and the fundamental substances in organisms, which can maintain acid-base balance and normal physiological activities. Na^+ and K^+ are essential for generating and transmitting nerve signals and muscle activities. The rapid and portable detection of Na^+ and K^+ is crucial in bioelectronics [39, 40]. OECTs, as ion-responsive electronic devices, are known for their low operating voltage and sensitive response to voltage changes [41]. While there have been numerous reports of OECTs detecting ion concentration [42], there are still some challenges with OECTs cation sensing. Firstly, the current chemical sensing predominantly relies on PEDOT:PSS-based OECTs, but the energy consumption problem of the depletion mode devices is limiting further development [15]. Secondly, the voltage response of p-type OECTs originates from anionic entry into the channel, which is contradictory to cation detection. N-type accumulation mode OECTs respond to cation doping and are more suitable for cation detection [27]. Given the OECT performance of fullerene derivatives in terms of response time and transconductance, we demonstrate PC4TEG-based OECTs sensing for Na^+ and K^+ concentration and ion-selective detection.

The OECT transfer and output curves of PC4TEG are characterized with 0.1 M NaCl(aq) and 0.1 M KCl(aq) as electrolytes, as shown in Fig. S21 in the ESM. The PC4TEG OECTs (channel length = 100 μm and channel width = 5 mm) have a stable current response with a maximum current response $I_D > 10^5$ A and a switching current ratio $I_{on/off} > 10^2$. The rapid and stable change in current indicates that the metal cations can smoothly enter the PC4TEG. When using OECTs as ion sensors, it is important to maintain stable current during operation to minimize the impact of disturbances other than ion concentrations. To ensure stability, we select V_G = 1 V and V_D = 0.6 V as the working voltage for subsequent ion sensing, based on the saturation region of the output curve. The stability of OECT operation in an aqueous environment is crucial for ion sensing. The rapid change in voltage pulses replicates the constant change in effective voltage acting on the channel caused by ion concentrations in real-world scenarios. Figure S16 in the ESM demonstrates that PC4TEG OECTs can continuously operate for 5000 cycles under rapid voltage switching.

We initially measure the device's current response in the absence of an ion-selective membrane (ISM), using 100 μM NaCl (aq) and KCl(aq) as the background, and then gradually introduce solutions of different concentrations after the currents have stabilized. In Fig. S22(a) in the ESM, the response of PC4TEG OECTs to continuously varying concentrations of NaCl and KCl solutions ranging from 100 μM to 1 M is demonstrated. As the concentration of the tested solution increased, the current change displays a gradual and steady upward step. Since the response speed of the OECTs is primarily limited by ion motion, the device is held for 50 s after each concentration change to reach a steady current. The current change at drain ΔI_D is used to monitor the ion concentration change in the solution. The sensitivities of PC4TEG OECTs to Na^+ and K^+ are separately extracted, as shown in Figs. S22(b) and S22(c) in the ESM. The current change displays a good linear relationship with the ion concentration range from 10 mM to 1 M. The sensitivity is 17.55 ± 0.93 μA·dec^{-1} for Na^+ and 8.09 ± 0.38 μA·dec^{-1} for K^+.

In practical ion sensing scenarios, precise detection of specific ions is often necessary. To verify the selectivity of our devices for Na^+, we mount a Na^+ ISM on PC4TEG OECTs. The sandwich structure of the ion-selective sensor is depicted in Fig. 5(a): The Na^+ ISM is placed above the channel, and a 0.1 M NaCl solution serves as the filling solution between the ISM and the channel. Figure 5(b) illustrates the comparison of the current response of the OECTs to Na^+ and K^+ after introducing the Na^+ ISM. In the same concentration range of 10 mM to 1 M, the current changes caused

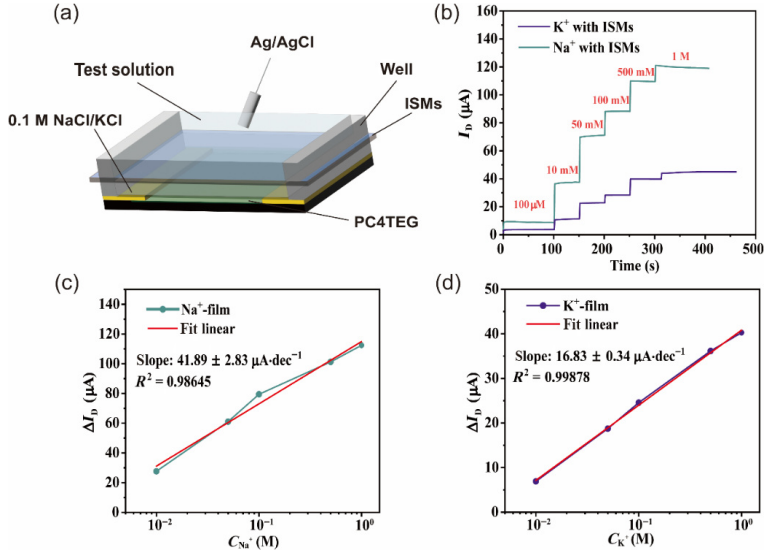

Figure 5 (a) Schematic diagram of a device with an ISM. (b) The current response of ion sensing tests using ISMs with varying NaCl and KCl aqueous concentrations ranging from 100 μM to 1 M. (c) and (d) The values of current changes in response to different concentrations of ions with ISM and their corresponding fitted curves.

by Na^+ are approximately three times higher than those caused by K^+. The data show a Na^+ sensitivity of 41.89 ± 2.83 μA·dec^{-1} and a K^+ sensitivity of 16.83 ± 0.34 μA·dec^{-1}, which is more than two times higher for Na^+ than for K^+, with $R^2 > 0.98$ indicating a good linear fit. These results demonstrate the excellent selectivity of the PC4TEG OECT towards Na^+ after incorporating a Na^+-selective film.

3 Conclusions

Side-chain engineering on OMIECs is a pivotal strategy for enhancing the performance of OECTs. In this study, we synthesize four fullerene derivatives with varying alkyl spacer lengths between fullerene and EG chains. PC4TEG and PC6TEG OECTs with appropriate alkyl spacers improve OECTs transconductance and volumetric capacitance by one magnitude, compared with the fullerene with only EG chain. Further increasing the alkyl spacer length results in non-functional device. The GIWAXS shows that PC4TEG and PC6TEG have larger intermolecular spacing, which may facilitate ion penetration. The volumetric capacitance of PC4TEG is 406.77 F·cm^{-3}, and PC6TEG is 569.49 F·cm^{-3}. However, alkyl groups' hydrophobic nature obstructs the movement of hydrated ions. Our investigation indicates the appropriate amphipathic side chains balance intermolecular spacing and ion motion, leading to optimized performance of OECTs. The enhanced transconductance is beneficial for amplifying the sensing signal in biological applications (the inverter displayed in Fig. S23 in the ESM). We have demonstrated that our OECTs are capable of selectively detecting Na^+ by employing a Na^+ ISM, with nearly three times higher sensitivity than K^+. This gives us confidence in using n-type OECTs for cation sensing in the future.

4 Experimental

4.1 Materials

Chloroform, NaCl, and KCl were purchased from Sigma–Aldrich. Tetrahydrofuran and valinomycin were obtained from Shanghai Acmec. High-molecular-weight polyvinyl chloride (PVC) and sodium tetrakis[3,5-bis(trifluoromethyl)phenyl] borate (Na-TFPB) were bought from Shanghai Aladdin. Bis(2-ethylehexyl) sebacate (DOS) was procured from Shanghai Titan. All chemicals were used as received.

4.2 OECT fabrication and characterization

The polymer solutions were dissolved in chloroform at a concentration of 5 mg·mL^{-1}. The interdigitated microelectrodes IDA-Au-6 were purchased from MicruX technologies with channel length 5 μm, number of pairs 30, and individual channel width 1.8 mm. The interdigitated microelectrodes were treated with UV zone for 20 min, following polymer solution spin-coating on it with 1000 rpm for 30 s and annealing at 100 °C for 30 min. The electrical characterization of devices was measured and recorded in 0.1 M NaCl solution covering the channel using a NI 1460 sourcemeter and Keithley 2612B. The transient response time was measured by waveform generator applying a 0–1 V pulsed voltage (with 3 Hz for PTEG-1, 3 Hz for PC4TEG, and 0.5 Hz for PC6TEG) to the gate of devices. At the same time, the sourcemeter applied the V_D and measured the I_D.

4.3 Cyclic voltammetry

The electrochemical workstation CHI760E (Shanghai Chenhua Instrument Co., Ltd) was used to conduct CV measurement. Spin-coated small molecule films on ITO glass were used as working electrodes. Three-electrode single-compartment cell was employed at 0.1 V·s^{-1} scanning rate from 0 to −0.8 V (vs. Ag/AgCl) with Pt sheet as couple electrodes and Ag/AgCl as reference electrodes in 0.1 M NaCl(aq).

4.4 Electrochemical impedance spectra

EIS measurement was performed on the polymer-coated Au electrodes using a three-terminal set-up and the electrochemical workstation CHI760E (Shanghai Chenhua Instrument Co., Ltd). Polymer was coated on Φ = 0.7 mm gold electrodes with Si substrate which was patterned by the lithography technique. The polymer coated gold electrodes were employed as working electrodes followed by the employment of Pt sheet as couple electrodes and Ag/AgCl as reference electrodes in 0.1 M NaCl solutions. The AC amplitude of voltage in form of sine-wave on the working electrodes was set as 10 mV with a frequency range

between 0.1 Hz to 100 kHz. The obtained dates were fitted to the Kovac's circuit.

4.5 Grazing incidence wide-angle X-ray scattering characterization

Two-dimensional (2D) GIWAXS was measured on a GANESHA 300XL+ system from JJ X-ray equipped with a Pilatus 300K detector, with a pixel size of 75 μm × 75 μm. The X-ray source was a Genix three-dimensional (3D) microfocus sealed tube X-ray Cu-source with an integrated monochromator (multilayer optic "3D version" optimized for SAXS) (30 W). The X-ray wavelength used was 1.54189 Å. The detector model was Dectris EIGER2 Si 500K. Date of corresponding line cut was processing via Fit 2D.

4.6 Spectroelectrochemistry measurements

Electrochemical spectroscopic measurements were tested by UV absorption spectrometer and electrochemical workstation CHI760E (Shanghai Chenhua Instrument Co., Ltd). Spin-coating of fullerene derivatives on ITO to prepare thin film samples was used as working electrodes.

4.7 Water contact angle measurement

The contact angle was measured by the angle of water on the fullerene film of ITO glass using the CA100 instrument of Guang Dong Hokuto Instrument Co.

4.8 Ion sensor device preparation

The ionic sensors used gold electrodes vaporized on the glass substrate with channel length of 100 μm and width of 0.5 mm. The current changes of the sensors caused by tested solutions were recorded by the timed current method. The Na^+ selective membrane was prepared from Na ionophore X (1% w/w), Na-TFPB (0.55% w/w), PVC (33% w/w), and DOS (65.45% w/w). 100 mg of the mixture was dissolved in 660 μL of tetrahydrofuran. The ion-selective membrane was formed by spin-coating the solution onto a glass substrate. The ion-selective membrane was placed between the reservoir and the tested solution, and the reservoir was filled with 0.1 M NaCl/KCl(aq).

Electronic Supplementary Material: Supplementary material (material synthesis, detailed thin film characterization data and additional OECT device characterization data) is available in the online version of this article at https://doi.org/10.26599/NR.2025.94907149.

Data availability

All data needed to support the conclusions in the paper are presented in the manuscript and the Electronic Supplementary Material. Additional data related to this paper may be requested from the corresponding author upon request.

Acknowledgements

We acknowledge funding from the National Natural Science Foundation of China (Nos. 22303071 and 51962036).

Declaration of competing interest

All the contributing authors report no conflict of interests in this work.

Author contribution statement

W. X. F.: Data curation, validation, writing manuscript, experimental design. Z. J. L.: Data curation, validation, writing manuscript, experimental design. C. D. W.: Data curation, validation, writing manuscript, experimental design. X. W. Z.: Data curation, validation, writing manuscript, experimental design. J. Y. L.: Data curation, validation, writing manuscript, experimental design. G. Y.: Writing manuscript, experimental design. F. W. H.: Writing manuscript, project administration, experimental design. Q. L.: Writing manuscript, project administration, experimental design, funding acquisition. Y. X. Z.: Writing manuscript, project administration, experimental design, funding acquisition. W. H.: Writing manuscript, project administration, experimental design. All the authors have approved the final manuscript.

Use of AI statement

None.

References

[1] Liu, F. Y.; Deswal, S.; Christou, A.; Sandamirskaya, Y.; Kaboli, M.; Dahiya, R. Neuro-inspired electronic skin for robots. *Sci. Robot.* **2022**, *7*, eabl7344.

[2] Gkoupidenis, P.; Zhang, Y.; Kleemann, H.; Ling, H.; Santoro, F.; Fabiano, S.; Salleo, A.; van de Burgt, Y. Organic mixed conductors for bioinspired electronics. *Nat. Rev. Mater.* **2024**, *9*, 134–149.

[3] Andersen, R. A.; Aflalo, T.; Bashford, L.; Bjånes, D.; Kellis, S. Exploring cognition with brain-machine interfaces. *Annu. Rev. Psychol.* **2022**, *73*, 131–158.

[4] Tan, S. T. M.; Gumyusenge, A.; Quill, T. J.; LeCroy, G. S.; Bonacchini, G. E.; Denti, I.; Salleo, A. Mixed ionic-electronic conduction, a multifunctional property in organic conductors. *Adv. Mater.* **2022**, *34*, 2110406.

[5] Tropp, J.; Meli, D.; Rivnay, J. Organic mixed conductors for electrochemical transistors. *Matter* **2023**, *6*, 3132–3164.

[6] Yao, Y.; Huang, W.; Chen, J. H.; Liu, X. X.; Bai, L. B.; Chen, W.; Cheng, Y. H.; Ping, J. F.; Marks, T. J.; Facchetti, A. Flexible and stretchable organic electrochemical transistors for physiological sensing devices. *Adv. Mater.* **2023**, *35*, 2209906.

[7] Liu, R. P.; Zhu, X. Y.; Duan, J. Y.; Chen, J. X.; Xie, Z.; Chen, C. Y.; Xie, X.; Zhang, Y. X.; Yue, W. Versatile neuromorphic modulation and biosensing based on n-type small-molecule organic mixed ionic-electronic conductors. *Angew. Chem., Int. Ed.* **2024**, *63*, e202315537.

[8] Chouhdry, H. H.; Lee, D. H.; Bag, A.; Lee, N. E. A flexible artificial chemosensory neuronal synapse based on chemoreceptive ionogel-gated electrochemical transistor. *Nat. Commun.* **2023**, *14*, 821.

[9] Xu, X. Z.; Zhang, H. Q.; Shao, L.; Ma, R.; Guo, M.; Liu, Y. Q.; Zhao, Y. An aqueous electrolyte gated artificial synapse with synaptic plasticity selectively mediated by biomolecules. *Angew. Chem., Int. Ed.* **2023**, *62*, e202302723.

[10] Chen, K.; Hu, H.; Song, I.; Gobeze, H. B.; Lee, W. J.; Abtahi, A.; Schanze, K. S.; Mei, J. G. Organic optoelectronic synapse based on photon-modulated electrochemical doping. *Nat. Photon.* **2023**, *17*, 629–637.

[11] Matrone, G. M.; Van Doremaele, E. R. W.; Surendran, A.; Laswick, Z.; Griggs, S.; Ye, G.; McCulloch, I.; Santoro, F.; Rivnay, J.; van de Burgt, Y. A modular organic neuromorphic spiking circuit for retina-inspired sensory coding and neurotransmitter-mediated neural pathways. *Nat. Commun.* **2024**, *15*, 2868.

[12] Harikesh, P. C.; Yang, C. Y.; Tu, D. Y.; Gerasimov, J. Y.; Dar, A. M.; Armada-Moreira, A.; Massetti, M.; Kroon, R.; Bliman, D.; Olsson, R. et al. Organic electrochemical neurons and synapses with ion mediated spiking. *Nat. Commun.* **2022**, *13*, 901.

[13] Sarkar, T.; Lieberth, K.; Pavlou, A.; Frank, T.; Mailaender, V.; McCulloch, I.; Blom, P. W. M.; Torricelli, F.; Gkoupidenis, P. An organic artificial spiking neuron for *in situ* neuromorphic sensing and biointerfacing. *Nat. Electron.* **2022**, *5*, 774–783.

[14] Ohayon, D.; Druet, V.; Inal, S. A guide for the characterization of organic electrochemical transistors and channel materials. *Chem. Soc. Rev.* **2023**, *52*, 1001–1023.

[15] Rivnay, J.; Inal, S.; Salleo, A.; Owens, R. M.; Berggren, M.; Malliaras, G. G. Organic electrochemical transistors. *Nat. Rev. Mater.* **2018**, *3*, 17086.

[16] Maria, I. P.; Griggs, S.; Rashid, R. B.; Paulsen, B. D.; Surgailis, J.; Thorley, K.; Le, V. N.; Harrison, G. T.; Combe, C.; Hallani, R. et al. Enhancing the backbone coplanarity of n-type copolymers for higher electron mobility and stability in organic electrochemical transistors. *Chem. Mater.* **2022**, *34*, 8593–8602.

[17] Moser, M.; Hidalgo, T. C.; Surgailis, J.; Gladisch, J.; Ghosh, S.; Sheelamanthula, R.; Thiburce, Q.; Giovannitti, A.; Salleo, A.; Gasparini, N. et al. Side chain redistribution as a strategy to boost organic electrochemical transistor performance and stability. *Adv. Mater.* **2020**, *32*, 2002748.

[18] Maria, I. P.; Paulsen, B. D.; Savva, A.; Ohayon, D.; Wu, R. H.; Hallani, R.; Basu, A.; Du, W. Y.; Anthopoulos, T. D.; Inal, S. et al. The effect of alkyl spacers on the mixed ionic-electronic conduction properties of n-type polymers. *Adv. Funct. Mater.* **2021**, *31*, 2008718.

[19] Duan, J. Y.; Zhu, G. M.; Lan, L. Y.; Chen, J. X.; Zhu, X. Y.; Chen, C. Y.; Yu, Y. P.; Liao, H. L.; Li, Z. K.; McCulloch, I. et al. Electron-deficient polycyclic molecules via ring fusion for n-type organic electrochemical transistors. *Angew. Chem., Int. Ed.* **2023**, *62*, e202213737.

[20] Tan, E.; Kim, J.; Stewart, K.; Pitsalidis, C.; Kwon, S.; Siemons, N.; Kim, J.; Jiang, Y. F.; Frost, J. M.; Pearce, D. et al. The role of long-alkyl-group spacers in glycolated copolymers for high-performance organic electrochemical transistors. *Adv. Mater.*, **2022**, *34*, 2202574.

[21] Griggs, S.; Marks, A.; Meli, D.; Rebetez, G.; Bardagot, O.; Paulsen, B. D.; Chen, H.; Weaver, K.; Nugraha, M. I.; Schafer, E. A. et al. The effect of residual palladium on the performance of organic electrochemical transistors. *Nat. Commun.* **2022**, *13*, 7964.

[22] Tang, H. R.; Liang, Y. Y.; Liu, C. C.; Hu, Z. C.; Deng, Y. F.; Guo, H.; Yu, Z. D.; Song, A.; Zhao, H. Y.; Zhao, D. Y. et al. A solution-processed n-type conducting polymer with ultrahigh conductivity. *Nature* **2022**, *611*, 271–277.

[23] Duan, J. Y.; Zhu, G. M.; Chen, J. X.; Zhang, C. Y.; Zhu, X. Y.; Liao, H. L.; Li, Z. K.; Hu, H. L.; McCulloch, I.; Nielsen, C. B. et al. Highly efficient mixed conduction in a fused oligomer n-type organic semiconductor enabled by 3D transport pathways. *Adv. Mater.* **2023**, *35*, 2300252.

[24] Sun, H. D.; Vagin, M.; Wang, S. H.; Crispin, X.; Forchheimer, R.; Berggren, M.; Fabiano, S. Complementary logic circuits based on high-performance n-type organic electrochemical transistors. *Adv. Mater.* **2018**, *30*, 1704916.

[25] Wang, X.; Zhang, Z.; Li, P. Y.; Xu, J. C.; Zheng, Y. T.; Sun, W. X.; Xie, M. Y.; Wang, J. R.; Pan, X. R.; Lei, X. et al. Ultrastable n-type semiconducting fiber organic electrochemical transistors for highly sensitive biosensors. *Adv. Mater.* **2024**, *36*, 2400287.

[26] Lei, Y. Q.; Li, P. Y.; Zheng, Y. T.; Lei, T. Materials design and applications of n-type and ambipolar organic electrochemical transistors. *Mater. Chem. Front.* **2024**, *8*, 133–158.

[27] Wu, W. C.; Feng, K.; Wang, Y. M.; Wang, J. W.; Huang, E. M.; Li, Y. C.; Jeong, S. Y.; Woo, H. Y.; Yang, K.; Guo, X. G. Selenophene substitution enabled high-performance n-type polymeric mixed ionic-electronic conductors for organic electrochemical transistors and glucose sensors. *Adv. Mater.* **2024**, *36*, 2310503.

[28] Savva, A.; Hallani, R.; Cendra, C.; Surgailis, J.; Hidalgo, T. C.; Wustoni, S.; Sheelamanthula, R.; Chen, X. X.; Kirkus, M.; Giovannitti, A. et al. Balancing ionic and electronic conduction for high-performance organic electrochemical transistors. *Adv. Funct. Mater.* **2020**, *30*, 1907657.

[29] Surgailis, J.; Flagg, L. Q.; Richter, L. J.; Druet, V.; Griggs, S.; Wu, X. C.; Moro, S.; Ohayon, D.; Kousseff, C. J.; Marks, A. et al. The role of side chains and hydration on mixed charge transport in *n*-type polymer films. *Adv. Mater.* **2024**, *30*, 2313121.

[30] Chen, S. E.; Flagg, L. Q.; Onorato, J. W.; Richter, L. J.; Guo, J. J.; Luscombe, C. K.; Ginger, D. S. Impact of varying side chain structure on organic electrochemical transistor performance: A series of oligoethylene glycol-substituted polythiophenes. *J. Mater. Chem. A* **2022**, *10*, 10738–10749.

[31] Yu, S. M.; Kousseff, C. J.; Nielsen, C. B. n-Type semiconductors for organic electrochemical transistor applications. *Synth. Met.* **2023**, *293*, 117295.

[32] Takeya, J.; Yamagishi, M.; Tominari, Y.; Hirahara, R.; Nakazawa, Y.; Nishikawa, T.; Kawase, T.; Shimoda, T.; Ogawa, S. Very high-mobility organic single-crystal transistors with in-crystal conduction channels. *Appl. Phys. Lett.* **2007**, *90*, 102120.

[33] Anthopoulos, T. D.; Kooistra, F. B.; Wondergem, H. J.; Kronholm, D.; Hummelen, J. C.; de Leeuw, D. M. Air-stable n-channel organic transistors based on a soluble C_{84} fullerene derivative. *Adv. Mater.* **2006**, *18*, 1679–1684.

[34] Bischak, C. G.; Flagg, L. Q.; Yan, K. R.; Li, C. Z.; Ginger, D. S. Fullerene active layers for n-type organic electrochemical transistors. *ACS Appl. Mater. Interfaces* **2019**, *11*, 28138–28144.

[35] Stein, E.; Nahor, O.; Stolov, M.; Freger, V.; Petruta, I. M.; McCulloch, I.; Frey, G. L. Ambipolar blend-based organic electrochemical transistors and inverters. *Nat. Commun.* **2022**, *13*, 5548.

[36] Kousseff, C. J.; Halaksa, R.; Parr, Z. S.; Nielsen, C. B. Mixed ionic and electronic conduction in small-molecule semiconductors. *Chem. Rev.* **2022**, *122*, 4397–4419.

[37] Liu, J.; Shi, Y. Q.; Dong, J. J.; Nugraha, M. I.; Qiu, X. K.; Su, M. Y.; Chiechi, R. C.; Baran, D.; Portale, G.; Guo, X. G. et al. Overcoming coulomb interaction improves free-charge generation and thermoelectric properties for n-doped conjugated polymers. *ACS Energy Lett.* **2019**, *4*, 1556–1564.

[38] Giridharagopal, R.; Flagg, L. Q.; Harrison, J. S.; Ziffer, M. E.; Onorato, J.; Luscombe, C. K.; Ginger, D. S. Electrochemical strain microscopy probes morphology-induced variations in ion uptake and performance in organic electrochemical transistors. *Nat. Mater.* **2017**, *16*, 737–742.

[39] Han, S.; Yamamoto, S.; Polyravas, A. G.; Malliaras, G. G. Microfabricated ion-selective transistors with fast and super-nernstian response. *Adv. Mater.* **2020**, *32*, 2004790.

[40] Li, T.; Cheryl Koh, J. Y.; Moudgil, A.; Cao, H.; Wu, X. H.; Chen, S.; Hou, K. Q.; Surendran, A.; Stephen, M.; Tang, C. et al. Biocompatible ionic liquids in high-performing organic electrochemical transistors for ion detection and electrophysiological monitoring. *ACS Nano* **2022**, *16*, 12049–12060.

[41] Sessolo, M.; Rivnay, J.; Bandiello, E.; Malliaras, G. G.; Bolink, H. J. Ion-selective organic electrochemical transistors. *Adv. Mater.* **2014**, *26*, 4803–4807.

[42] Liu, H.; Song, J. J.; Zhao, Z. Y.; Zhao, S. Q.; Tian, Z. Y.; Yan, F. Organic electrochemical transistors for biomarker detections. *Adv. Sci.* **2024**, *11*, 2305347.